ChemComm

COMMUNICATION

View Article Online
View Journal

Check for updates

Cite this: DOI: 10.1039/d4cc01331j

Received 22nd March 2024,
Accepted 29th April 2024

DOI: 10.1039/d4cc01331j

rsc.li/chemcomm

Published on 30 April 2024. Downloaded by University of Rochester on 5/16/2024 8:48:43 PM.

O_2 reduction *via* proton-coupled electron transfer by a V(III) aquo on a polyoxovanadate-alkoxide cluster†

Shannon E. Cooney, ‡ Eric Schreiber, ‡ Baela M. Ferrigno and Ellen M. Matson *

We report the transfer of H-atoms from a reduced polyoxovanadate alkoxide $[^n Oct_4N][V_6O_6(OH_2)(OMe)_{12}]$ *via* concerted proton–electron transfer. Oxygen reduction is compared between bridging and terminal O–H bonds revealing similar mechanisms, providing new insight to design criteria for metal-oxide electrocatalysts that faciliate oxygen reduction by concerted-proton electron transfer.

Hydrogen fuel cells (HFCs) are promising technologies for renewable electrical energy due to their lack of carbon emissions. With the paired employment of the hydrogen oxidation and oxygen reduction reactions (HOR and ORR, respectively), electrical energy is generated with water as the sole waste product. ORR is considered the bottleneck to the widespread adoption of HFCs due to its sluggish kinetics.[1,2] Currently, to meet performance levels necessary for HFC technologies, high loadings of precious metal catalysts (typically Pt) are required, rendering these systems prohibitively expensive.[3] Thus, the development of inexpensive, high-performing cathode materials is necessary.

An alternative class of catalysts that has been demonstrated to facilitate ORR are reducible metal oxides (MO_x).[4–6] Despite the library of oxides competent for ORR, the scale and heterogeneity of MO_x renders direct mechanistic determination of the net $4H^+/4e^-$ reaction challenging, hindering further advances in the optimization (*e.g.* efficiency, selectivity) of MO_x derived catalysts.

To study metal oxide-mediated small molecule activation chemistries with atomic precision, our lab and others have turned to a class of molecular analogues called polyoxometalates (POMs).[7–11] These clusters feature similar composition and surface structure to nanoscopic and bulk MO_x, rendering them ideal platforms for the investigation of reactions and mechanisms at MO_x surfaces. With respect to the ORR, it is well established that exposure of reduced POMs to air results in cluster re-oxidation.[12,13] However, relatively little is known about the mechanism(s) of ORR at the surface of these assemblies.[14] A notable example of ORR by a reduced POM comes from Weinstock and coworkers, where a reduced, Keggin-type polyoxotungstate, $[AlW_{12}O_{40}]^{6-}$, reduces O_2 *via* proton-coupled electron transfer (PCET).[15] The multi-site PCET to form H_2O_2 occurs by initial electron transfer from the cluster, followed by proton transfer from the acidic surrounding media (ET-PT). Subsequent work from our laboratory demonstrated the use of a $6H^+/6e^-$ reduced complex, $[V_6O_7(OH)_6(TRIS^{NO2})_2]^{2-}$, (Fig. 1) for ORR to H_2O in acetonitrile through a series of concerted proton–electron transfer (CPET) steps.[16]

Recently, we reported the *in situ* generation of a reduced POV-alkoxide *via* addition of two H-atom equivalents to $[^n Oct_4N][V_6O_7(OMe)_{12}]$ ($\mathbf{1\text{-}V_6O_7}^{1-}$), yielding a cluster hypothesized to feature a terminal V^{III}–OH_2, $[^n Oct_4N][V_6O_6(OH_2)(OMe)_{12}]^{1-}$ ($\mathbf{2\text{-}V_6O_6(OH_2)}^{1-}$; Scheme 1).[17] The $BDFE(O–H)_{avg}$ values of $\mathbf{2\text{-}V_6O_6(OH_2)}^{1-}$ are similar to the reported values for the bridging hydroxides of $[V_6O_7(OH)_6(TRIS^{NO2})_2]^{2-}$ (59.9 and 61.6 kcal mol^{-1}, respectively), rendering the thermodynamics of small molecule hydrogenation comparable for these clusters despite the disparate sites at which their reducing equivalents are stored (*e.g.* terminal aquo *vs.* bridging hydroxide).[16,17] We thus became interested in understanding the reactivity of $\mathbf{2\text{-}V_6O_6(OH_2)}^{1-}$ toward small molecule hydrogenation reactions, as comparison of the reactivity between the two systems would provide an opportunity to examine the effect of the location of surface O–H moieties on the mechanism and kinetics of PCET from POV-alkoxides.

Complex $\mathbf{2\text{-}V_6O_6(OH_2)}^{1-}$ can be isolated by addition of an equivalent of 5, 10-dihydrophenazine to $\mathbf{1\text{-}V_6O_7}^{1-}$ in THF.[17,18] The ^1H NMR spectrum of the product features an asymmetric feature at 26.0 ppm and a symmetrical signal at −14.9 ppm;

Department of Chemistry, University of Rochester, Rochester NY 14627, USA. E-mail: ellen.matson@rochester.edu

† Electronic supplementary information (ESI) available: Synthetic and other experimental procedures, spectroscopic data, kinetic analyses for the oxidation of $\mathbf{2\text{-}V_6O_6(OH_2)}^{1-}$ with TEMPO and O_2. See DOI: https://doi.org/10.1039/d4cc01331j

‡ SEC and ES contributed equally to this work.

Published on 30 April 2024. Downloaded by University of Rochester on 5/16/2024 8:48:43 PM.

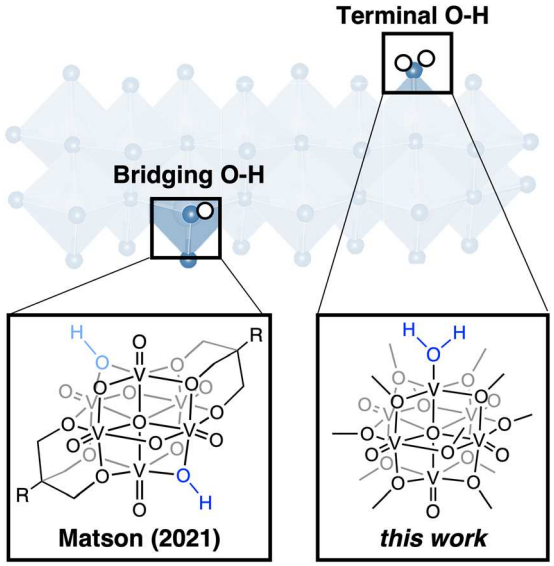

Fig. 1 H-atom uptake at POV-alkoxide clusters that model MO_x surfaces. Reducing equivalents can be isolated to bridging and terminal oxide sites at the surface of POV-alkoxides. Blue spheres represent O-atoms, and white spheres represent H-atoms.

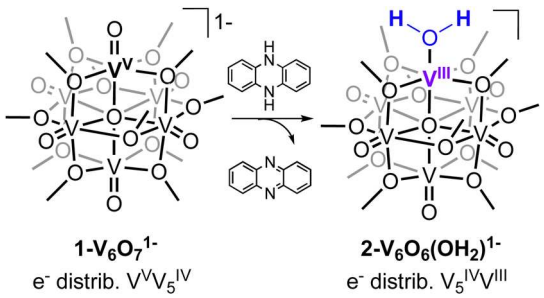

Scheme 1 Synthesis of **2-$V_6O_6(OH_2)^{1-}$**.

these features are consistent with reduction in cluster symmetry upon formation of a site-differentiated V^{III} center (Fig. S1, ESI†).[19,20] Analogous reactions performed on the 1e$^-$ oxidized cluster, $V_6O_7(OMe)_{12}$, have been shown to result in formation of a POV-alkoxide bearing a single V^{III}–OH_2 moiety, $V_6O_6(OH_2)(OMe)_{12}$.[21] Attempts to obtain crystals of **2-$V_6O_6(OH_2)^{1-}$** were unsuccessful due to the greasy counterion required to maintain solubility of the aquo-ligated cluster in THF. Thus, we rely on the following spectroscopic and reactivity analyses to support the formation of the terminal aquo.

The infrared (IR) spectrum of **2-$V_6O_6(OH_2)^{1-}$** reveals features corresponding to the O–CH_3 and V=O stretching modes (1042 and 953 cm^{-1}, respectively; Fig. S2, ESI†). An additional broad, weak band at 3429 cm^{-1} is observed, assigned to the O–H stretch of the bound water molecule. We note that this feature is not present in IR spectrum of the MeCN adduct of the O-atom deficient assembly, $[V_6O_6(MeCN)(OMe)_{12}]^{1-}$.[19] Additional evidence of the delivery of two H-atom equivalents to the cluster surface is observed upon inspection of the electronic absorption spectra (EAS) of the POV-alkoxide clusters (Fig. S3, ESI†).[18] The parent cluster, **1-$V_6O_7^{1-}$**, has a prominent feature in the near-IR region (λ_{max} = 1265 nm, ε = 937 M^{-1} cm^{-1}), due to intervalence charge transfer (IVCT) between the V^{IV} and V^{V} in the assembly. This band is quenched upon 2e$^-$/2H$^+$ reduction, with the only NIR band being a weak d–d transition at 1010 nm (ε = 138 M^{-1} cm^{-1}). The absorption spectrum of the reduced assembly possesses a transition at 519 nm (ε = 1137 M^{-1} cm^{-1}), with an extinction coefficient that is significantly greater than the corresponding band of $[V_6O_6(MeCN)(OMe)_{12}]^{1-}$ (λ_{max} = 518 nm; ε = 180 M^{-1} cm^{-1}). We suggest that intensity of this band is related to the changes in ligand field imparted by the aquo on the d–d transition. Finally, the presence of a terminal aquo moiety is confirmed from the reaction of **2-$V_6O_6(OH_2)^{1-}$** with MeCN, which results in the release of water molecules, observed by ^{1}H NMR spectroscopy, as MeCN preferentially binds to the reduced vanadium centre (Fig. S4, ESI†).

Having successfully generated the aquo-ligated POV-alkoxide, we next turned to H-atom transfer from **2-$V_6O_6(OH_2)^{1-}$**. TEMPO (2,2,6,6-tetramethyl-1-piperidinyloxy), (TEMPO-H BDFE(O–H) = 65.5 kcal mol^{-1}), serves as an excellent model for H-atom abstraction due to the substrate being difficult to reduce, and unlikely to be protonated by the moderately basic **2-$V_6O_6(OH_2)^{1-}$**.[18,22,23] This leaves the most likely pathway for oxidation of **2-$V_6O_6(OH_2)^{1-}$** as CPET. Exposure of two equivalents of TEMPO to **2-$V_6O_6(OH_2)^{1-}$** results in quantitative formation of **1-$V_6O_7^{1-}$**, as indicated by ^{1}H NMR spectroscopy (Fig. S5 and S6, ESI†). Kinetic investigations were performed by monitoring the reaction progression *via* EAS, through the method of initial rates (see ESI† for more information). The reaction is found to proceed through a rate determining step that is first order in cluster, **2-$V_6O_6(OH_2)^{1-}$**, and first order in

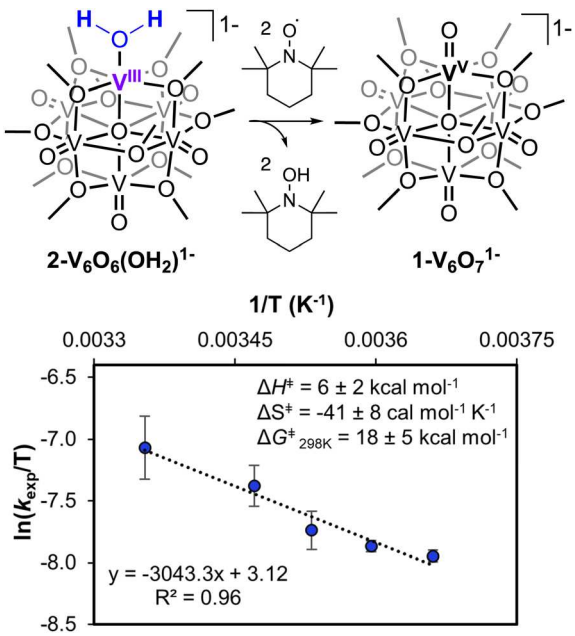

Fig. 2 Oxidation by TEMPO (top), Eyring plot for the reaction of 0.30 mM **2-$V_6O_6(OH_2)^{1-}$** and 10 mM TEMPO, 0–25 °C.

This journal is © The Royal Society of Chemistry 2024

Published on 30 April 2024. Downloaded by University of Rochester on 5/16/2024 8:48:43 PM.

TEMPO with an overall experimentally derived rate constant of 0.15 ± 0.01 M^{-1} s^{-1} (Fig. S7–S10; see ESI† for more details).

Next, we conducted variable temperature kinetic experiments to determine the activation parameters for the oxidation of **2-$V_6O_6(OH_2)^{1-}$** by TEMPO (Fig. 2). These experiments have been shown to be valuable for assessing mechanisms of PCET reactions (Fig. S11, ESI†).[24–27] For the oxidation of **2-$V_6O_6(OH_2)^{1-}$**, a large and negative value for the entropy of activation ($\Delta S^{\ddagger}$ = −41 ± 8 cal mol K^{-1}) is consistent with an ordered, bimolecular, H-bonded intermediate invoked in CPET mechanisms.[18,27–30] Accordingly, the small enthalpy of activation ($\Delta H^{\ddagger}$ = 6 ± 2 kcal mol^{-1}), which falls within a range of similar $\Delta H^{\ddagger}$ values reported for CPET in other metal oxide complexes, suggests stabilization by an H-bonded complex in the activated state.[18,24–28] These studies demonstrate that **2-$V_6O_6(OH_2)^{1-}$** is capable of transferring H-atoms *via* CPET.

After establishing the mechanism of H-atom transfer from **2-$V_6O_6(OH_2)^{1-}$** as CPET, we investigated the reactivity and mechanism of cluster-mediated O_2 reduction. Exposure of **2-$V_6O_6(OH_2)^{1-}$** to 1 atm of O_2 results in quantitative formation of **1-$V_6O_7^{1-}$** and water, as confirmed by ^{1}H NMR spectroscopy (Fig. S12, ESI†). In our work investigating ORR by $[V_6O_7(OH)_6(TRIS^{NO2})_2]^{2-}$, H_2O_2 was observed prior to the formation of water. Similarly, for **2-$V_6O_6(OH_2)^{1-}$**, at early time points (~80 s), we observe a signal at 9.37 ppm as the cluster is oxidized, which is consumed by 910 s (Fig. S13, ESI†). To confirm the assignment of this resonance as H_2O_2, we performed trapping experiments using triphenylphosphine (PPh_3).[31,32] Importantly, PPh_3 is unreactive toward O_2 and **1-$V_6O_7^{1-}$** under these conditions, meaning any $OPPh_3$ formation is solely due to the presence of H_2O_2 produced *in situ* (Fig. S14–S17, ESI†).[20] Upon exposure of cluster to O_2 in the presence of PPh_3, the generation of $OPPh_3$ is observed, suggesting that ORR by **2-$V_6O_6(OH_2)^{1-}$** proceeds through an H_2O_2 intermediate.

H_2O_2 formation upon exposure of **2-$V_6O_6(OH_2)^{1-}$** to O_2 is made possible due to the relative strength of the O–H bonds formed in the product ($BDFE(O–H)_{avg}$ = 69 kcal mol^{-1} in water) in comparison with those of **2-$V_6O_6(OH_2)^{1-}$**.[23] Evidence of H_2O_2 is suggestive that substrate activation is proceeding through PCET from the V^{III}–OH_2 moiety.[23] This result differs to prior work from our laboratory that has described the mechanism of reoxidation of O-atom deficient POV-alkoxide clusters by O_2 as proceeding through a Mars-van-Krevelen-type mechanism.[19,33] Following this route, bifurcation of the O–O bond through interaction of the substrate with an exposed V^{III} site (formed following the dissociation of solvent) results in oxidation of the assembly.

We next turned to kinetic analyses to elucidate the mechanism of ORR by **2-$V_6O_6(OH_2)^{1-}$**. ORR was monitored by EAS, following the procedure described previously (Fig. 3 and Fig. S18–S22; see ESI† for details). To determine the order with respect to **2-$V_6O_6(OH_2)^{1-}$**, we performed reactions under pseudo-first order conditions by adding an excess of O_2 (Fig. 3, inset). Results suggest a rate expression for ORR described as: rate = k_{exp}[**2-$V_6O_6(OH_2)^{1-}$**]^1[O_2]^1. From the intercept of the line, the experimentally derived second order rate constant, k_{exp}, can be extracted (k_{exp} = 0.061 ± 0.008 M^{-1} s^{-1}). The observed rate for ORR by **2-$V_6O_6(OH_2)^{1-}$** is significantly accelerated compared to the MeCN bound assembly, $V_6O_6(MeCN)(OMe)_{12}^{1-}$, which is oxidized over the course of 8 days (Fig. S23, ESI†).

Next, we considered the possible mechanisms of H-atom transfer from the cluster to O_2. Initial proton transfer to O_2 is thermodynamically disfavoured.[34] Instead, transfer of a net H-atom (H^+/e^-) to O_2 occurs through either CPET or ET-PT. Such stepwise mechanisms are invoked for catalysts that enable ORR; initial ET is observed by either an outer or inner-sphere mechanism to form $O_2^{\bullet-}$, followed by protonation by the surrounding solvent media.[34] However, in the case of **2-$V_6O_6(OH_2)^{1-}$**, we observed no evidence of ET. *In situ* analysis of the reaction progression following addition of O_2 to **2-$V_6O_6(OH_2)^{1-}$** by ^{1}H NMR spectroscopy shows no formation of the one electron oxidized **2-$V_6O_6(OH_2)^{1-}$**, $V_6O_6(OH_2)(OMe)_{12}^{0}$ (Fig. S13, ESI†). This is consistent with the fact that **2-$V_6O_6(OH_2)^{1-}$** lacks sufficient driving force (E_{ox} = −0.67 V *vs.* $Fc^{+/0}$) to readily perform ET to O_2 (E_{Red} = −1.25 V *vs.* $Fc^{+/0}$).[21,35] We consequently propose that ORR by **2-$V_6O_6(OH_2)^{1-}$** occurs *via* a rate limiting CPET from the V^{III}–OH_2 terminus.

There are limited examples of O_2 reduction *via* CPET; however, ORR by **2-$V_6O_6(OH_2)^{1-}$** is reminiscent of the mechanism previously investigated by our group for $[V_6O_7(OH)_6(TRIS^{NO_2})_2]^{2-}$.[16] These POV-alkoxides are unique because they facilitate ORR from

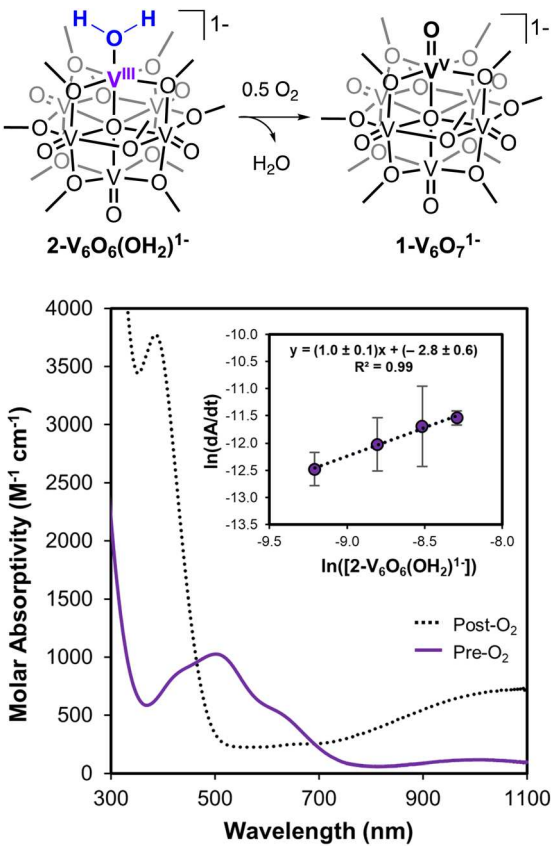

Fig. 3 Initial and final EAS scans for the oxidation of **2-$V_6O_6(OH_2)^{1-}$**. Inset shows log–log plot of the rate *versus* [**2-$V_6O_6(OH_2)^{1-}$**].

Published on 30 April 2024. Downloaded by University of Rochester on 5/16/2024 8:48:43 PM.

adsorbed H-atoms on the cluster surface. We therefore attribute CPET reactivity to the H^+/e^- originating from the same bond (*i.e.* bridging hydroxide or terminal aquo). This observed preference for CPET ORR by both **2-$V_6O_6(OH_2)^{1-}$** and $[V_6O_7(OH)_6(TRIS^{NO2})_2]^{2-}$ may be credited to the thermodynamic preference to avoid energetically costly charged intermediates, a consequence of strong thermodynamic coupling of the proton and electron. Additionally, while at first glance the rates of ORR by the two POV-alkoxides seem similar, considering the number of available H-atoms available to react with O_2 (2 for **2-$V_6O_6(OH_2)^{1-}$** and 6 for $[V_6O_7(OH)_6(TRIS^{NO_2})_2]^{2-}$), the aquo-bound complex in fact reacts $\sim$4 times faster (1.8×10^{-5} M s^{-1} and 5.0×10^{-6} M s^{-1}). This acceleration could be accounted for by the driving forces for $2H^+/2e^-$ transfer to O_2; ORR by **2-$V_6O_6(OH_2)^{1-}$** is 1.5 kcal mol^{-1} more thermodynamically downhill, though we cannot rule out the effect of site-specific reactivity in accelerating the rate. The H-atoms in $[V_6O_7(OH)_6(TRIS^{NO_2})_2]^{2-}$ are located across the six equatorial bridging oxides of the Lindqvist core, meaning that an O_2 molecule would need to migrate between each CPET step. By localizing both reducing equivalents to the same site, ORR at **2-$V_6O_6(OH_2)^{1-}$** requires little to no movement of O_2, accelerating the reaction. Therefore, by generating bound H-atoms at terminal or bridging sites on MO_x surfaces, accelerated ORR rates may be accessed by pushing reaction mechanisms toward CPET.

Here, the terminal V^{III}–OH_2 site on **2-$V_6O_6(OH_2)^{1-}$** is found to be capable of mediating hydrogenation reactions *via* CPET for small molecule substrates (*e.g.* TEMPO, O_2). After establishing reactivity, we employ our POV-alkoxide clusters as molecular models for ORR to explore the effect of H-atoms bound at bridging *vs.* terminal oxide sites. Ultimately, both O–H sites yield CPET mediated ORR, suggesting that adsorbed H-atoms dictate the preferred mechanism. This work presents a new synthetic strategy to improve ORR by incorporating bound H-atoms on the surface of MO_x.

This research was funded by the National Science Foundation (CHE-2154727). B. M. F. performed investigations with TEMPO, all other experiments were performed by S. E. C and E. S. All authors contributed to the writing of the manuscript. We acknowledge Dr. Kamaless Patra for kinetic discussions and Kathryn R. Proe for assistance in data collection.

Conflicts of interest

There are no conflicts to declare.

Notes and references

1 Y. He, S. Liu, C. Priest, Q. Shi and G. Wu, *Chem. Soc. Rev.*, 2020, **49**, 3484–3524.
2 R. Lin, X. Cai, H. Zeng and Z. Yu, *Adv. Mater.*, 2018, **30**, 1705332.
3 M. Shao, Q. Chang, J.-P. Dodelet and R. Chenitz, *Chem. Rev.*, 2016, **116**, 3594–3657.
4 W. T. Hong, M. Risch, K. A. Stoerzinger, A. Grimaud, J. Suntivich and Y. Shao-Horn, *Energy Environ. Sci.*, 2015, **8**, 1404–1427.
5 Y. Wang, J. Li and Z. Wei, *J. Mater. Chem. A*, 2018, **6**, 8194–8209.
6 C. Goswami, K. K. Hazarika and P. Bharali, *Mater. Sci. Energy Technol.*, 2018, **1**, 117–128.
7 S. Chakraborty, B. E. Petel, E. Schreiber and E. M. Matson, *Nanoscale Adv.*, 2021, **3**, 1293–1318.
8 D.-L. Long, E. Burkholder and L. Cronin, *Chem. Soc. Rev.*, 2007, **36**, 105–121.
9 D.-L. Long, R. Tsunashima and L. Cronin, *Angew. Chem., Int. Ed.*, 2010, **49**, 1736–1758.
10 Y.-F. Song and R. Tsunashima, *Chem. Soc. Rev.*, 2012, **41**, 7384–7402.
11 M. T. Pope and A. Müller, *Angew. Chem., Int. Ed. Engl.*, 1991, **30**, 34–48.
12 C. W. Anson and S. S. Stahl, *Chem. Rev.*, 2020, **120**, 3749–3786.
13 M. R. Horn, A. Singh, S. Alomari, S. Goberna-Ferrón, R. Benages-Vilau, N. Chodankar, N. Motta, K. Ostrikov, J. MacLeod, P. Sonar, P. Gomez-Romero and D. Dubal, *Energy Environ. Sci.*, 2021, **14**, 1652–1700.
14 I. V. Kozhevnikov, Y. V. Burov and K. I. Matveev, *Bull. Acad. Sci. USSR, Div. Chem. Sci.*, 1981, **30**, 2001–2007.
15 Y. V. Geletii, C. L. Hill, R. H. Atalla and I. A. Weinstock, *J. Am. Chem. Soc.*, 2006, **128**, 17033–17042.
16 A. A. Fertig, W. W. Brennessel, J. R. McKone and E. M. Matson, *J. Am. Chem. Soc.*, 2021, **143**, 15756–15768.
17 C. Y. M. Peter, E. Schreiber, K. R. Proe and E. M. Matson, *Dalton Trans.*, 2023, **52**, 15775–15785.
18 S. E. Cooney, A. A. Fertig, M. R. Buisch, W. W. Brennessel and E. M. Matson, *Chem. Sci.*, 2022, **13**, 12726–12737.
19 B. E. Petel, W. W. Brennessel and E. M. Matson, *J. Am. Chem. Soc.*, 2018, **140**, 8424–8428.
20 B. E. Petel and E. M. Matson, *Chem. Commun.*, 2020, **56**, 13477–13490.
21 S. E. Cooney, E. Schreiber, W. W. Brennessel and E. M. Matson, *Inorg. Chem. Front.*, 2023, **10**, 2754–2765.
22 E. Schreiber, W. W. Brennessel and E. M. Matson, *Inorg. Chem.*, 2022, **61**, 4789–4800.
23 R. G. Agarwal, S. C. Coste, B. D. Groff, A. M. Heuer, H. Noh, G. A. Parada, C. F. Wise, E. M. Nichols, J. J. Warren and J. M. Mayer, *Chem. Rev.*, 2022, **122**, 1–49.
24 P. Mondal, I. Ishigami, E. F. Gérard, C. Lim, S.-R. Yeh, S. P. de Visser and G. B. Wijeratne, *Chem. Sci.*, 2021, **12**, 8872–8883.
25 O. Snir, Y. Wang, M. E. Tuckerman, Y. V. Geletii and I. A. Weinstock, *J. Am. Chem. Soc.*, 2010, **132**, 11678–11691.
26 T. H. Parsell, M.-Y. Yang and A. S. Borovik, *J. Am. Chem. Soc.*, 2009, **131**, 2762–2763.
27 J. Amtawong, B. B. Skjelstad, D. Balcells and T. D. Tilley, *Inorg. Chem.*, 2020, **59**, 15553–15560.
28 E. Schreiber, A. A. Fertig, W. W. Brennessel and E. M. Matson, *J. Am. Chem. Soc.*, 2022, **144**, 5029–5041.
29 N. Kindermann, C.-J. Günes, S. Dechert and F. Meyer, *J. Am. Chem. Soc.*, 2017, **139**, 9831–9834.
30 T. G. Carrell, P. F. Smith, J. Dennes and G. C. Dismukes, *Phys. Chem. Chem. Phys.*, 2014, **16**, 11843–11847.
31 A. Chellmani and R. Suresh, *React. Kinet. Catal. Lett.*, 1988, **37**, 501–505.
32 A. S. Ivanova, A. D. Merkuleva, S. V. Andreev and K. A. Sakharov, *Food Chem.*, 2019, **283**, 431–436.
33 R. L. Meyer, P. Miró, W. W. Brennessel and E. M. Matson, *Inorg. Chem.*, 2021, **60**, 13833–13843.
34 M. L. Pegis, C. F. Wise, D. J. Martin and J. M. Mayer, *Chem. Rev.*, 2018, **118**, 2340–2391.
35 D. Vasudevan and H. Wendt, *J. Electroanal. Chem.*, 1995, **392**, 69–74.

 This journal is © The Royal Society of Chemistry 2024